Q-switching bifurcation dynamics of passively mode-locked lasers

N. Akhmediev[1] and J. M. Soto-Crespo[2]
[1]*Department of Theoretical Physics, Research School of Physics, The Australian National University, Canberra ACT 2600, Australia*
[2]*Instituto de Óptica CSIC, Serrano 121, 28006 Madrid, Spain*

(Received 9 June 2021; accepted 10 August 2021; published 26 August 2021)

We model *Q*-switched pulses in passively mode-locked lasers using the cubic-quintic complex Ginzburg-Landau equation (CGLE). We show that a wide set of parameters of this equation leads to *Q*-switched pulses of triangular shape that consist of a periodic sequence of evolving dissipative solitons. Bifurcation diagrams demonstrating various transformations of these pulses are calculated in terms of five major parameters of the CGLE. The diagrams show period doubling transformations as well as the transition to a chaotic evolution of the *Q*-switched pulses.

DOI: 10.1103/PhysRevE.104.024221

I. INTRODUCTION

Passive mode locking [1–4] and passive *Q* switching [5–8] are two optical pulse generating techniques tightly related to each other [9]. In each case, a saturable absorber is an essential part of the laser cavity [10–13]. This device, responsible for the internal self-modulation of the cavity finesse, leads to the pulse generation. In the case of mode locking, these pulses are individual dissipative solitons (DSs) [14–17] while in the case of *Q* switching, they are amplitude modulated sequences of dissipative solitons [18–20]. Two consequences of such relation are, first, the duration of the *Q*-switched pulses is much longer than the duration of mode-locked pulses and, second, both type of pulses can be modeled using similar tools [21].

The cubic-quintic complex Ginzburg-Landau equation (CGLE) is a useful equation for modeling a variety of passively mode-locked lasers. When used for a qualitative analysis of pulse generation by these devices, the CGLE has proved to be capable of predicting very specific laser dynamics that are normally beyond the reach of other modeling tools. Examples of such predictions include exploding solitons [22–24], multisolitons [25], dissipative soliton resonances (DSR) [26,27], creeping solitons [22,28,29], bifurcations of solitons [24,30,31], and chaotic solitons [24]. These effects were first found in numerical simulations, and their existence has been fully confirmed experimentally [32–35]. Therefore, further studies of the CGLE may produce new results of practical importance. The brightest example of practical use of the CGLE is the DSR phenomenon, which is now a popular technique for high-energy pulse generation [36–39].

The standard form of the CGLE has six parameters that roughly correspond to physical effects within the laser cavity. Variation of these parameters leads to dissipative soliton solutions just as the variation of the laser parameters leads to the generation of short pulses of different shapes. A correspondence between both can be established by comparing the pulse shapes and their changes when varying the parameters. The presence of six parameters in the theoretical model and about the same in the experiments makes the task highly complicated. Finding new types of pulses and their classification in theory is a formidable exercise. Despite these difficulties, a significant progress has been reached and several qualitatively different types of DSs and the areas of their existence have been identified so far.

In all previous works, the CGLE has been used for a qualitative analysis of passively mode-locked lasers. However, it was shown, recently, that the power of this technique can be expanded to cover a much larger variety of laser systems [40]. Namely, even passively *Q*-switched lasers can be analyzed based on the solutions of the CGLE. A preliminary analysis and the comparison with experimental data demonstrating this possibility have been provided in [40]. In the present work, we present more numerical simulations that support our claims made in [40]. In particular, we expand the range of parameters of the CGLE that has DS solutions that can be interpreted as *Q*-switched pulses.

The CGLE describes both, the effects of dissipative soliton formation in each round trip, and the effects of soliton evolution from one round trip to another when the DS is not stationary. The most common DS evolution is a nearly sinusoidal change of the soliton parameters over many round trips [30]. This can be considered as one form of the *Q*-switching dynamics [18]. However, this is not the only possible form. Another form is a *Q*-switched pulse of triangular shape with a sharp peak at the maximum [41]. This form needs more careful studies as it was observed experimentally [40,42,43]. Moreover, the dynamics of these pulses is more complex than being simply periodic. It includes the cases when two, or more, such pulses per period with unequal amplitudes are involved in the evolution [41]. This phenomenon has also been observed in [40,43]. In the present work, we extend the parameter space where these type of pulses can be observed. Every parameter of the CGLE has been varied in order to see the change of the pulse shape and the bifurcations leading to different pulse sequence transformations.

II. *Q*-SWITCHED PULSES IN THE CGLE MODEL

For modeling passively Q-switched lasers, we use the cubic-quintic complex Ginzburg-Landau equation. The parameters of this equation can be related to the parameters of laser systems [44,45]. This relation is a separate task that requires a detailed analysis of each particular laser. Our goal here is presenting our results in a general form that can be applied to a multiplicity of lasers with various designs that include fiber, solid state, and semiconductor lasers. Thus, for numerical simulations, we use the CGLE, which in its standard form reads [30]

$$i\psi_z + \frac{D}{2}\psi_{\tau\tau} + |\psi|^2\psi + \nu|\psi|^4\psi = i\delta\psi + i\beta\psi_{\tau\tau} + i\epsilon|\psi|^2\psi + i\mu|\psi|^4\psi, \quad (1)$$

where ψ is the envelope of the optical field, D the average cavity dispersion, and ν a higher-order nonlinear coefficient. The dissipative terms in the right-hand side of Eq. (1) include δ which is the linear loss or gain parameter, ϵ which represents the cubic gain or loss, and μ which is the gain saturation. The parameter β is the spectral cavity bandpass coefficient. The τ variable is the time within each round trip moving with the pulse, while the z-variable is a continuous variable linearly proportional to the number of round trips. The passive mode-locking device in this model does not have any time delay function, i.e., all processes in the cavity are fast. The coefficients δ, ϵ, and μ are greatly influenced by this device. Dissipative solitons exist when $\delta < 0$, $\epsilon > 0$, and $\mu < 0$.

For numerical simulations of Eq. (1) we have used a split-step technique with a fourth-order Runge-Kutta algorithm for solving the nonlinear part of the equation, while the linear part was solved in Fourier space. In most cases, the step size along the z-axis was taken to be 10^{-6}. Multiplying or dividing this step size by 2 did not change the outcome indicating that it was sufficiently small to provide accurate results. The number of mesh points along the τ-axis varied from 65 536 to more than a a million in order to provide sufficient space for solitons with tails decaying to zero in both time and frequency domains. The largest windows have been used for solutions pulsating with very high amplitudes.

The soliton energy $Q = \int |\psi|^2 d\tau$ within the computation box has been calculated using a trapezoidal rule. The accuracy of our numerical modeling was sufficient to provide six significant digits for the Q-value. Increasing or decreasing the step size in τ twice did not change these six digits. Bifurcation diagrams presented below have been calculated with steps along β, δ, and ϵ lesser or equal to 0.001. Parameters ν and μ that are smaller, required increments of 0.0001.

For finding the soliton solutions, we fixed the equation parameters and used sech-type initial conditions localized at the center of the numerical window. When the width and the amplitude of the sech function are close to those of the solution, we observed its convergence to the soliton solution. In most cases, the basin of attraction around the soliton is remarkably large, and the convergence to the solution occurred relatively quickly even for large deviations of the initial profile from the actual soliton shape. Once one solution is found, we used it as initial condition for the next set of parameters. This is a convenient technique for finding the bifurcation diagrams

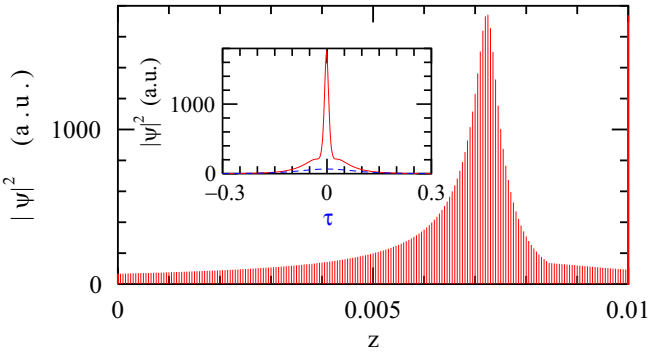

FIG. 1. Example of a single Q-switched pulse that consists of a train of dissipative solitons. The vertical red bars show the maximal intensity, $|\psi|^2$, of each DS. The inset shows the pulse profiles of the DS pulses at the maximum (red solid line) and minimum (blue dashed line) of the Q-switched pulse. For a particular choice of $\Delta z = 0.0005$, as explained in the text, there are 200 round trips (DSs) along the horizontal axis.

when only one of the equation parameters is changed in small increments. This technique mimics the experimental approach when one experimental parameter (say the pump) is changed in small steps with the resulting change of the pulse profile in the cavity.

One example of the soliton profile obtained this way is shown in the inset in Fig. 1. The soliton is pulsating, and its shape changes from one extremal profile to the other. The profile with the highest amplitude is shown by the red curve while the profile with the lowest amplitude is shown by the blue dashed curve. The change of the soliton amplitude at its center along the z-axis is depicted by discrete red vertical lines in Fig. 1.

The DS generated inside the fiber cavity is observed by coupling a small fraction of the circulating pulse as the output at certain place in the cavity, thereby transforming a single DS circulating in the cavity into a train of pulses. The pulses in the train are separated by the round trip time T. When the DS changes from one round trip to another, the train becomes modulated and appears in the form of a longer pulse. Then this longer pulse is a passively Q-switched pulse. In order to illustrate the above idea, we present in Fig. 1 one of the Q-switched pulses that consists of a periodic train of DSs separated by the cavity round trip time T. Parameters of the CGLE are specified as follows: $\epsilon = 1.5$, $\delta = -10.8$, $\beta = 0.3$, $D = 0.9$, $\mu = -0.001$, and $\nu = 0.004$. This set of parameters is chosen because it produces the typical Q-switched pulses we are interested in. Changing slightly any one of these parameters separately keeps the pulse shape similar to the one shown in Fig. 1. This set of parameters actually leads to two different pulses in a period. Only one of them is shown here as the second one has a similar shape but slightly different width and amplitude. The separations between pulses are also different and depend on the equation parameters.

The horizontal axis, z, in Fig. 1 is linearly proportional to the number of round trips. Let us call the change of the z variable in one round trip as Δz. The value of Δz in constructing the plot in Fig. 1 serves as the scaling parameter for comparisons of these type of plots with experimental ones. A

typical Q-switched pulse in experiments consists of hundreds or thousands of DSs [18,42,43]. In order to stay in this range, Δz in Fig. 1 is chosen to be 0.00005. This corresponds to 200 round trips along the z-axis in Fig. 1 or 200 DSs as we assume that there is only one soliton in each round trip. This means that outside the cavity, time is measured by replacing Δz by T. The DSs are represented by the red vertical bars in this figure and the actual profiles of the dissipative solitons at the maximum and the minimum of the Q-switched pulse are shown in the inset.

The vertical axis in Fig. 1 represents the field intensity $|\psi|^2$. However, the DS intensity at its maximum is difficult to measure when the pulse duration is in the picosecond or femtosecond ranges. Then the total energy of such short pulses is its natural measure. The energy of a DS pulse generated within each round trip is

$$Q(z) = \int_{-T/2}^{T/2} |\psi(z,\tau)|^2 \, d\tau.$$

The pulse is usually much shorter than T and its amplitude decays exponentially to zero at its tails. Then the actual value of T is not essential and $Q(z)$ is the total energy per round trip. The average intensity of the train of DS pulses can be found by dividing the DS energy Q by the duration of the round trip time T:

$$I(z) = \frac{Q(z)}{T} = \frac{1}{T} \int_{-T/2}^{T/2} |\psi(z,\tau)|^2 \, d\tau.$$

The round trip time T is not explicitly present in the CGLE model. The soliton energy Q does not depend on T as its tails decay to zero at the end of this interval. However, the average intensity $I(z)$ does depend on T. Nevertheless, in most experiments, the measured average intensity is normally presented in arbitrary units, and therefore any linear coefficient can be ignored. Hence, the actual value of T does not influence the results. Up to an arbitrary coefficient, the intensity of the Q-switched pulse can be presented in terms of the energy Q of the conforming individual DSs. Consequently, this variable will be used in all data presented below.

Our results are obtained for solutions of Eq. (1) that have settled after the influence of the initial conditions has ceased. They show only stable stationary or Q-switched pulse solutions of the CGLE. In most of the cases, the solution found for the previous set of parameters has been used as initial condition for the next set of parameters that are close to the previous ones. This choice accelerates the process of finding the solutions. Generally, the stability of the DSs is an involved issue. It has previously been analyzed in detail [46,47] and will not be considered here. The convergence of an initial pulse to a certain state in the numerical simulations is sufficient for being confident with its stability.

III. BIFURCATION DIAGRAMS FOR EXTREMA OF Q-SWITCHED PULSES

In order to demonstrate that the type of Q-switching dynamics considered here occupies a large region in the parameter space, we vary them, one by one, around one particular point. In this way, we have constructed several bifurcation diagrams. Most of them are centered around the point in the parameter space that was used for constructing the Q-switched pulse in Fig. 1. We call it "the departure point" as in each step of exploration of the parameter space, we will be roaming around it, returning back and starting again in a different direction. It is a good starting point because the Q-switched pulse with "triangular" shape shown in Fig. 1 is typical for most of our simulations even if one of the parameters is changing. It is worth to mention again that the sequence of Q-switched pulses at this point is periodic with two slightly different pulses per period. This is also typical for sequences observed at the nearest neighborhood of this point. Deviations from this point in several directions leaves the pulse shapes qualitatively similar to the one shown in Fig. 1. However, the number of pulses per period with different amplitudes may change as soon as a bifurcation point is reached. These changes can be seen in the bifurcation diagrams presented below.

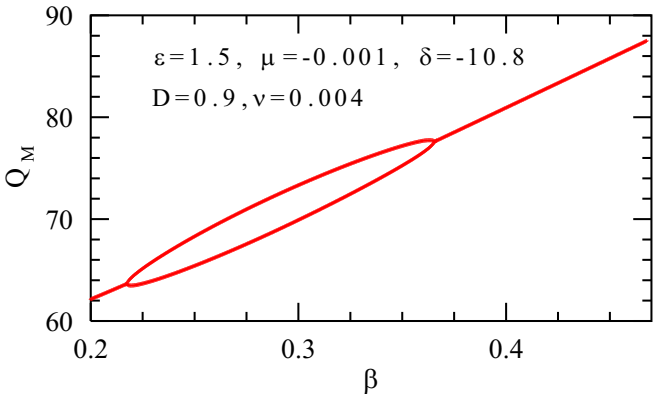

FIG. 2. Bifurcation diagram in β variable. Only the pulse maxima are shown. Two different pulses in a period are observed in the interval $0.22 < \beta < 0.37$.

There are six parameters in Eq. (1). Obviously, the total space cannot be covered by a single illustration. The best that could be done, would be diagrams in a three-dimensional space, when two equation parameters are changed. However, even these illustrations would be excessively cumbersome and would lose clarity because of the multiplicity of transitions along each of the two axes representing the two chosen equation parameters. Therefore, bidimensional diagrams are the best choice both for clarity and for having a general impression of all possible scenarios. Again, there is a limited number of such diagrams that can be presented within a single paper. Thus, we limit ourselves to the most representative ones that nevertheless illustrate the majority of the bifurcation types that we have observed.

When constructing these diagrams, we varied one of the parameters while fixing the other five. Figure 2 shows one such example. All parameters are the same as in the "departure point" except for β, which is varied in a relatively large interval. For convenience, the values of the five fixed parameters are written inside the figure while β is varied from 0.2 to 0.475. For the sake of higher resolution, the vertical axis is limited to the values covering only the branch of maximal values of the energy Q. Figure 2 shows that in the interval $0.22 < \beta < 0.37$ there are two such maxima that correspond

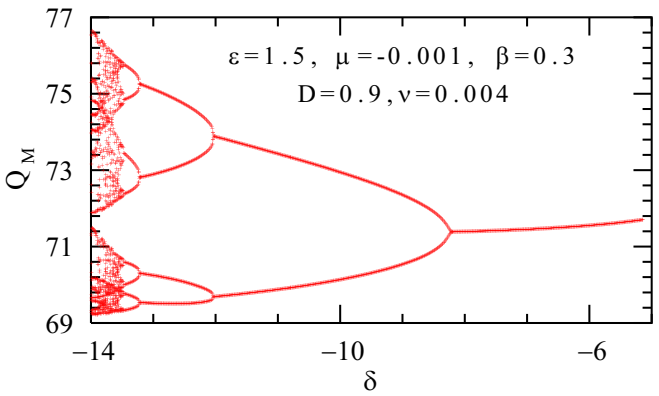

FIG. 3. Bifurcation diagram in δ variable. There is nearly a classic period doubling sequence as δ decreases. Four of the bifurcations of the sequence are clearly seen. The pulse generation becomes chaotic when $\delta \approx -13.5$.

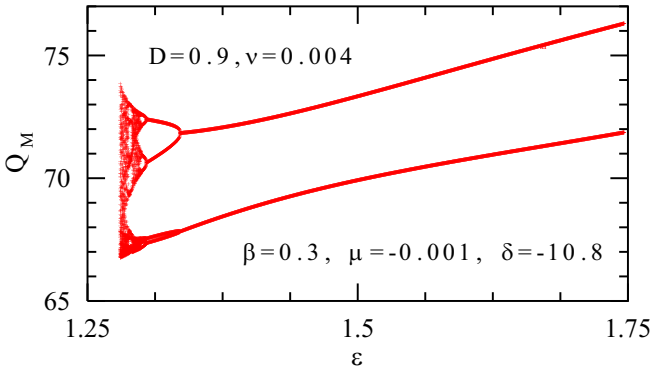

FIG. 4. Bifurcation diagram in ϵ variable. There are two pulses per period nearly in the whole interval shown here. Period quadrupling occurs at $\epsilon = 1.32$ and transition to chaos at the left part of the diagram.

to two Q-switched pulses per period just as in the departure point $\beta = 0.3$. Bifurcations at the two ends of this interval lead to a single pulse per period. In the rest of the range shown in Fig. 2 there is one pulse per period. At the left end of the interval shown in Fig. 2 the solitons become unstable and disappear. Consequently, this point also limits the range of existence of Q-switched pulses. The right-hand side of the plot extends almost linearly up to the point $\beta = 0.8$. (This part is not shown to keep a better resolution of the presented curves.) At the point $\beta = 0.8$ solitons and the related Q-switched pulses also vanish.

An important point that follows from this analysis is that the range of existence of Q-switched pulses in β-domain is very large. If we consider the departure point as the countdown position, this range covers the relative change of β from 66% of this value to 266%. In other words, β can be changed four times from its minimal value to its maximal one and the Q-switched pulses will continue to exist within this interval. As β characterizes the spectral width of the cavity transmission, such a big range should allow one to find easily the parameter range necessary for the observation of this phenomenon in experiments. Similar conclusion will be drawn when we consider other bifurcation diagrams.

Figure 3 shows the bifurcation diagram in the δ-variable. This plot confirms that the departure point chosen above ($\delta = -10.8$) corresponds to two pulses per period. To the right from this point, at $\delta = -8.2$, the two curves merge leading to a periodic evolution with a single pulse per period. However, to the left of this point, at $\delta = -12$, we observe a period quadrupling bifurcation and the sequence of several period doubling bifurcations leading to a chaotic dynamics. The maximal amplitude of the chaotic Q-switched pulse changes in the interval from $Q_M = 69$ to $Q_M = 77$ with the pulse separations also evolving chaotically. Thus, the interval $-14 < \delta < -13.5$ corresponds to the generation of a chaotic sequence of Q-switched pulses. At the right-hand side of the full interval shown in Fig. 3, at $\delta = -5.13$, the solitons enter a region of instability and disappear. Consequently, the Q-switched pulses also disappear.

The sequence of period doubling bifurcations in Fig. 3 resembles a similar effect in a logistic map [48]. However, such similarity should not be understood as a direct analogy. There is a drastic difference between the one-dimensional logistic map and an infinite dimensional system such as the CGLE [49]. Period doubling, tripling, etc., in this case are qualitatively different phenomena: here the whole function $\psi(t)$ changes its shape periodically rather a single number as in the case of a discrete logistic map. Second, the logistic map has only one variable parameter while the CGLE has six. The calculation of Lyapunov exponents or other related parameters for a soliton entering a chaotic regime is possible [49] but requires significant attention to the details. This task is far beyond the simple demonstration of the Q-switching effect that we present here.

Figure 4 shows the bifurcation diagram in the ϵ-variable. The departure point is located right in the middle of this diagram. Again, there are two pulses per period at this point. They exist to the right from this point up to $\epsilon = 1.75$. The energy Q_M increases with ϵ, as higher ϵ roughly corresponds to higher nonlinear gain. The two pulses exist also to the left of the departure point down until $\epsilon = 1.34$ which is the point of period quadrupling. Further decrease in ϵ leads to chaotic dynamics through a sequence of period doubling bifurcations. Leaving this part of the dynamics aside, we observe that the main feature of the effect such as two triangular pulses per period occupy the whole interval from $\epsilon = 1.34$ to $\epsilon = 1.75$ without any visible interruption. Taking into account that this is a nonlinear coefficient, the length of this interval ≈ 0.4 is, indeed, large. For experimental situations, this means that the effect could be found with relative ease.

The effect is highly sensitive to the changes of the parameter μ, as it represents the saturation of the nonlinear gain which is the quintic dissipative term. This is why we constructed three different bifurcation diagrams with μ as a variable. For these plots, we fixed the linear loss term to be $\delta = -10.8, -12$, and -15, respectively. This way, we cover a wider range of parameters in our simulations. Figure 5 is again constructed around the departure point with $\mu = -0.001$. As expected, there are two pulses per period at this point with the same values of Q_M as at the center of Fig. 4. The two maximal

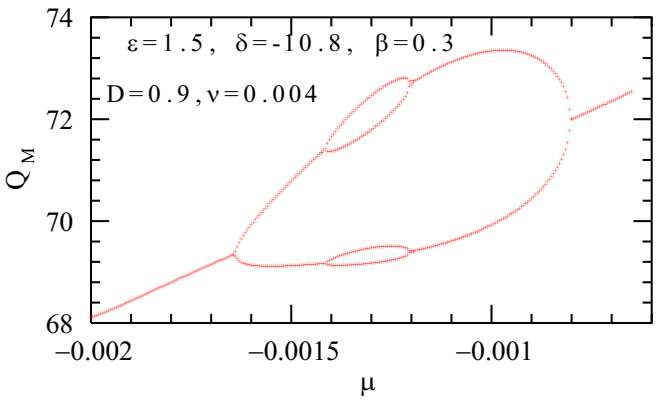

FIG. 5. Bifurcation diagram in μ variable that includes the departure point. There is a single pulse per period below $\mu = -0.00164$ and above $\mu = -0.0008$. Period doubling and period quadrupling are observed inside this interval.

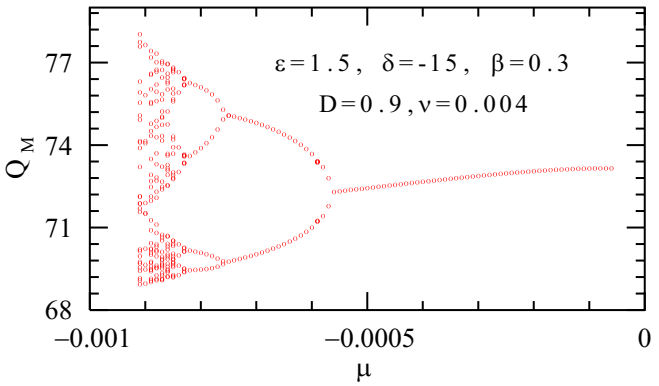

FIG. 7. Another bifurcation diagram in μ variable that does not include the departure point. Parameters are the same as in Fig. 5 except for δ which is now in the chaotic region in Fig. 3. Consequently, the transition to chaos appears in this diagram.

amplitudes Q_M merge to a single one at $\mu = -0.0009$, which is a bifurcation to a single pulse per period. There are four pulses per period in the interval of $-0.0014 < \mu < -0.0012$. This is the interval closest to chaotic behavior in the sense that if, for example, ϵ is decreased, the process may enter the sequence of period doubling bifurcations as in Fig. 4. Below this interval, the number of pulses per period is two up until the point $\mu = -0.00164$. Below this point, the two pulses become identical leading to a single pulse per period.

Figure 6 shows another bifurcation diagram similar to the one in Fig. 5 but now with $\delta = -12$. The plot in this figure does not include the departure point. The scale along the horizontal axis is also slightly different. It starts at the right-hand side from μ slightly below zero. Solutions with a single pulse per period exist up to $\mu = -0.00074$. This is not very far from the similar bifurcation point in Fig. 5. Period quadrupling bifurcation occurs at around $\mu = -0.001$. This is also not very far from the similar point in Fig. 5. In contrast to Fig. 5, we observe here the transition to period 8 solutions at $\mu = -0.00116$. This mode extends till $\mu = -0.0012$. However, solutions cease to exist to the left from this point. No transition to chaotic evolution can be observed. The range of μ shown in Fig. 6 covers the whole interval of solutions that we are studying.

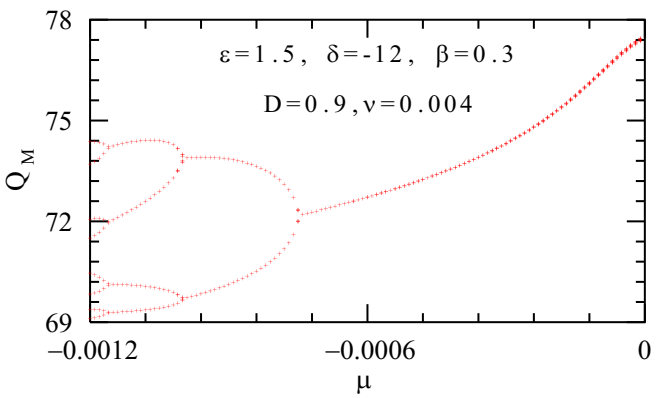

FIG. 6. Bifurcation diagram in μ variable that does not include the departure point. Parameters are the same as in Fig. 5 except for δ, which is now closer to the threshold of period quadrupling in Fig. 3. The whole diagram is shifted to the left, and a period octupling bifurcation appears now at $\mu = -0.00116$.

Even larger deviation form the departure point is chosen for constructing the bifurcation diagram in Fig. 7. Namely, in this case, $\delta = -15$. As a result, the diagram shows a route to chaos via a sequence of period doubling bifurcations. The first bifurcation point from a single pulse to two pulses per period occurs at $\mu = -0.00055$. There is an additional shift of this point in comparison to the diagram in Fig. 6. The second, period quadrupling bifurcation occurs at $\mu = -0.00076$. Full scale chaotic dynamics occurs at the left-hand side of the diagram. The solution vanishes completely (decays to zero) at around $\mu = -0.00092$.

In order to illustrate the transition from period two to period four in the bifurcation diagram in Fig. 7, we present two pulse sequences, that correspond to the points indicated by the green dashed vertical lines. These plots are shown in Fig. 8. The left panels show the pulse sequence with two pulses per period while the right panels show the sequence with four pulses per period. Although the shapes of the pulses are very similar, their amplitude, energy, Q, and separation are different. Nevertheless, the overall dynamics remains strictly periodic but the periods are different. The left panel shows two periods of evolution while the right panel shows only one. The pulse sequence in the next period is exactly the same as in the one shown in this figure. This figure clearly illustrates the period quadrupling bifurcation in the situation when the pulse shapes remain qualitatively the same as at the departure point. This is another convincing demonstration that the effect that we are studying occupies a large area in the parameter space of the CGLE.

The last parameter that we varied in our simulations is the quintic nonlinearity ν. The bifurcation diagram in ν variable is shown in Fig. 9. In contrast to the previous diagrams, here, we show both the maxima Q_M and minima Q_m of the pulse energy. The green curve shows the branch of stationary stable solitons with fixed amplitude. As we decrease ν stationary solitons increase its energy until they cease to exist at negative values of ν. At the opposite end of this branch, at

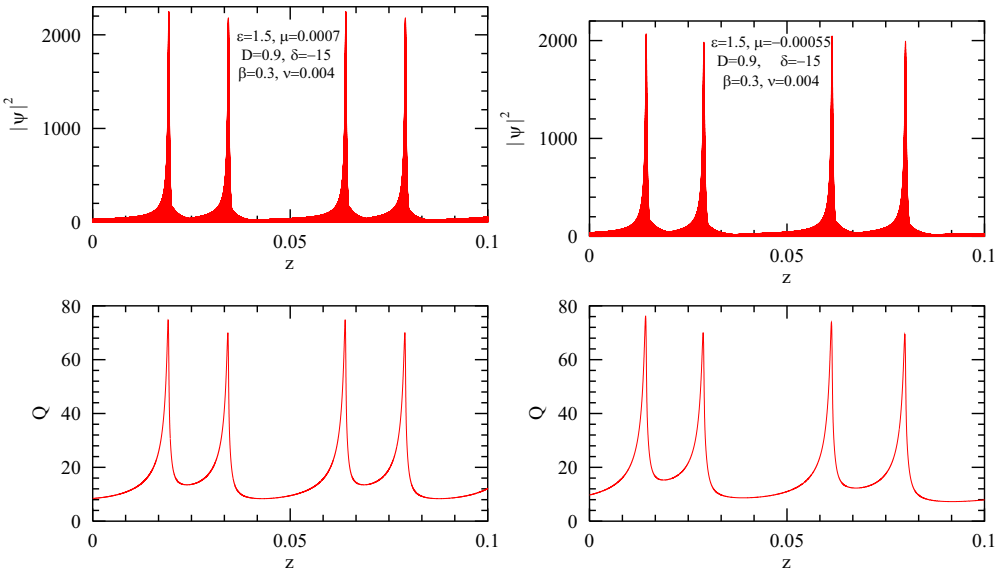

FIG. 8. Two examples of sequences of Q-switched pulses with (a) two and (b) four pulses per period. The amplitudes of the four pulses in (b) are slightly different, while the different separations between them are more evident. The upper panels show intensity $|\psi|^2$ while the lower panels show the pulse energy Q. The values of μ chosen here are highlighted by the green vertical dashed lines in Fig. 6. After crossing the bifurcation point, the number of pulses per period changes from two to four.

$\nu = 0.0029$, the stationary DSs are transformed into the train of solitons that is part of the Q-switched pulses with energy Q oscillating between Q_m and Q_M. Transition from the train of stationary solitons (the green curve) to Q-switched pulses (the red and blue curves) and vice versa is abrupt and includes a small region of hysteresis (not shown). Immediately after the transition, the Q-switched pulses have a single pulse per period. However, at the next bifurcation point, $\nu = 0.003$, which is very close to the previous one, the successive pulses become unequal leading to period doubling. This transition is seen as splitting of the two curves in Fig. 9. At higher values of ν, we can observe two intervals of period quadrupling.

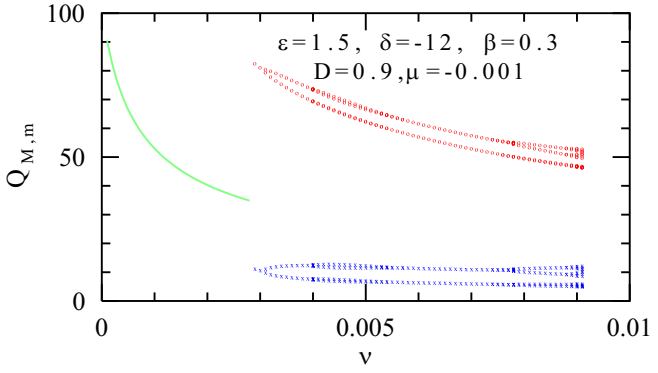

FIG. 9. Bifurcation diagram in ν variable. The green curve shows the branch of stationary stable dissipative solitons. At $\nu > 0.0029$, this branch becomes unstable and turns into the sequence of Q-switched pulses. The points of period doubling and period quadrupling bifurcations are located at $\nu = 0.003$, $\nu = 0.004$, $\nu = 0.0052$, and $\nu = 0.0076$. In contrast to the previous diagrams, here both the maxima Q_M (red curves) and minima Q_m (blue curves) of DS energy Q are shown.

Additional splitting of the curves corresponds to four pulses per period. This happens at the intervals $0.004 < \nu < 0.0053$ and $0.0078 < \nu < 0.0091$. Although the splitting of the maxima or minima in these intervals is very small, the effect still can be seen in the scale of Fig. 9. Dissipative solitons become unstable and completely disappear above the point $\nu = 0.0092$. As a result, the Q-switched pulses also disappear.

Parameters D and β are responsible for linear effects. They can be simultaneously rescaled and reduced to a single effective parameter β/D. Therefore, changing D produces similar bifurcation diagram as changing β. It is not given here. Thus, by varying only five parameters around the departure point we have obtained a sufficiently detailed qualitative pattern of bifurcations in the region of existence of triangular Q-switched pulses. Simultaneously, we have obtained rough estimates of the boundaries of this area as the ends of the intervals that we considered are essentially the limits of the existence of this type of Q-switched pulses.

We would like to stress that the triangular pulse shapes are in the z variable. Thus, they are Q-switched pulses that consist of a sequence of solitons with much shorter duration. In the τ variable, in all cases that we have considered, the pulses are nearly bell-shaped solitons with a single maximum and exponentially decaying tails. They change their amplitude and width but remain robust entities at the whole area of parameters that admit triangular Q-switched pulses.

IV. CONCLUSIONS

We have shown in this work that the whole area of the CGLE parameters admitting Q-switched pulses has been overlooked in previous publications. Here, and in [40], we have filled this gap in the knowledge of the immense world of the Ginzburg-Landau equation. The range of parameter change in our bifurcation diagrams reached the edges of existence of the

type of pulses that we studied. This fact shows that the region of their existence is very large. Nevertheless, we realize, that there may be other areas that also admit such type of pulses or pulses with other shapes. The work in this direction should be continued.

Clearly, the technique of modeling the Q-switched pulses offered in this work is only one of the existing possibilities. There are other modeling tools that are in use today [50–52]. Being a continuous one, our model may miss certain features of the phenomenon of Q switching that are related to the discreteness of the cavity dynamics. The discreteness can be taken into account in this model using periodically varying coefficients in the CGLE. There is a vast number of possibilities in extending the model to be more realistic. Our work can be considered as a starting point in this endeavor.

Comparison with experiments is a decisive step in these studies. The first work in this direction has been done in [40]. Continuation in this direction is also essential for further progress in modeling lasers with passive Q switching.

ACKNOWLEDGMENT

The work of J.M.S.C. is funded by Spanish MICINN Grant No. RTI2018-097957-B-C33, and Comunidad de Madrid Grant No. S2018/NMT-4326 SINFOTON2-CM.

[1] E. P. Ippen, Principles of passive mode locking, Appl. Phys. B **58**, 159 (1994).

[2] V. L. Kalashnikov, V. P. Kalosha, V. P. Mikhailov, I. G. Poloyko, and M. I. Demchuk, Efficient self-mode locking of continuous-wave solid-state lasers with resonant nonlinearity in an additional cavity, Opt. Commun. **109**, 119 (1994).

[3] R. Paschotta, R. Häring, A. Garnache, S. Hoogland, A. C. Tropper, and U. Keller, Soliton-like pulse shaping mechanism in passively mode-locked surface-emitting semiconductor lasers, Appl. Phys. B **75**, 445 (2002).

[4] H. Hassan, M. A. Munshid, and A. Al-Janabi, Tellurium-nanorod-based saturable absorber for an ultrafast passive mode-locked erbium-doped fiber laser, Appl. Opt. **59**, 1230 (2020).

[5] J. A. Morris and C. R. Pollock, Passive Q switching of a diode-pumped Nd:YAG laser with a saturable absorber, Opt. Lett. **15**, 440 (1990).

[6] D. Popa, Z. Sun, T. Hasan, F. Torrisi, F. Wang, and A. C. Ferrari, Graphene Q-switched, tunable fiber laser, Appl. Phys. Lett. **98**, 073106 (2011).

[7] C. Feng, B. Ma, W. Qiao, G. Li, J. Zhao, K. Yang, D. Li, G. Li, S. Zhao, and T. Li, Passively Q-switched Er:Lu_2O_3 laser at 2.8 μm with TiC saturable absorber, Appl. Opt. **59**, 8066 (2020).

[8] E. Beyatl, F. Kaya, and H. Bilici, Self-Q-switched and multicolor operation of a Tm:LuAG laser, Appl. Opt. **59**, 8247 (2020).

[9] C. Frerichs and U. B. Unrau, Passive Q-Switching and mode-locking of erbium-doped fluoride fiber lasers at 2.7 μm, Opt. Fiber Techn. **2**, 358 (1996).

[10] H. Li, H. Xia, C. Lan, C. Li, X. Zhang, J. Li, and Y. Liu, Passively Q-switched erbium-doped fiber laser based on few-layer MoS_2 saturable absorber, IEEE Photonics Technol. Lett. **27**, 69 (2014).

[11] D. E. Spence, P. N. Kean, and W. Sibbett, 60-fsec pulse generation from a self-mode-locked Ti:sapphire laser, Opt. Lett. **16**, 42 (1991).

[12] P. Wang, Y. Tang, H. Peng, G. Shi, T. He, H. Li, and Y. Liu, A long cavity passive mode-locking fibre laser with the reflective non-linear optical loop mirror, J. Modern Opt. **64**, 122 (2017).

[13] H. Ahmad, N. F. Azmy, F. a M. Kasran, N. Yusoff, S. A. Reduan, L. Bayang, M. F. Ismail, M. Z. Zulkifli, and K. Thambiratnam, Passively Q-switched S+/S band fiber laser with copper telluride saturable absorber, Laser Phys. Lett. **17**, 095102 (2020).

[14] N. Akhmediev and A. Ankiewicz, *Dissipative Solitons*, Lecture Notes in Physics (Springer, Berlin, 2005), Vol. 661.

[15] P. Grelu and N. Akhmediev, Dissipative solitons for mode-locked lasers, Nat. Photon. **6**, 84 (2012).

[16] W. Renninger, A. Chong, and F. Wise, Dissipative solitons in normal dispersion fiber lasers, Phys. Rev. A **77**, 023814 (2008).

[17] V. L. Kalashnikov, Chirped dissipative solitons of the complex cubic-quintic nonlinear Ginzburg-Landau equation, Phys. Rev. E **80**, 046606 (2009).

[18] S. Kimura, S. Tani, and Y. Kobayashi, Q-switching stability limits of Kerr-lens mode locking, Phys. Rev. A **102**, 043505 (2020).

[19] Y.-F. Chen and S. W. Tsai, Simultaneous Q-switching and mode-locking in a diode-pumped Nd:YVO/sub4-Cr/sub 4+/:YAG laser, IEEE J. Quantum Electron. **37**, 580 (2001).

[20] J. Liu, L. Li, S. Liu, Min Liu, and Y.-G. Wang, Passively Q-switched mode-locking of diode-pumped Nd:YVO_4 laser with GaAs intracavity absorber grown at low temperature, Eur. Phys. J. Appl. Phys. **39**, 233 (2007).

[21] X. Liu, D. Popa, and N. Akhmediev, Revealing the Transition Dynamics from Q Switching to Mode Locking in a Soliton Laser, Phys. Rev. Lett. **123**, 093901 (2019).

[22] J. M. Soto-Crespo, N. Akhmediev, and A. Ankiewicz, Pulsating, Creeping, and Erupting Solitons in Dissipative Systems, Phys. Rev. Lett. **85**, 2937 (2000).

[23] O. Descalzi, C. Cartes, J. Cisternas, and H. R. Brand, Exploding dissipative solitons: The analog of the Ruelle-Takens route for spatially localized solutions, Phys. Rev. E **83**, 056214 (2011).

[24] N. Akhmediev, J. M. Soto-Crespo, and G. Town, Pulsating solitons, chaotic solitons, period doubling, and pulse coexistence in mode-locked lasers: CGLE approach, Phys. Rev. E **63**, 056602 (2001).

[25] N. Akhmediev, A. Ankiewicz, and J. M. Soto-Crespo, Multisoliton Solutions of the Complex Ginzburg-Landau Equation, Phys. Rev. Lett. **79**, 4047 (1997).

[26] W. Chang, A. Ankiewicz, J. M. Soto-Crespo, N. Akhmediev, Dissipative soliton resonances, Phys. Rev. A **78**, 023830 (2008).

[27] Q. Gong, H. Zhang, D. Deng, and J. Zu, Dissipative soliton resonance in an all-polarization maintaining fiber laser with a nonlinear amplifying loop mirror, IEEE Phot. J. **12**, 1502708 (2020).

[28] Y. Zhang, Y. Cui, L. Huang, L. Tong, and X. Liu, Full-field real-time characterization of creeping solitons dynamics in a mode-locked fiber laser, Opt. Lett. **45**, 6246 (2020).

[29] S. C. V. Latas, M. F. S. Ferreira, and M. V. Facao, Characteristics of fixed-shape pulses emerging from pulsating, erupting, and creeping solitons, Appl. Phys. B **116**, 279 (2014).

[30] J. M. Soto-Crespo, M. Grapinet, Ph. Grelu, and N. Akhmediev, Bifurcations and multiple-period soliton pulsations in a passively mode-locked fiber laser, Phys. Rev. E **70**, 066612 (2004).

[31] D. Gomila, A. J. Scroggie, and W. J. Firth, Bifurcation structure of dissipative solitons, Physica D **227**, 70 (2007).

[32] S. T. Cundiff, J. M. Soto-Crespo, and N. Akhmediev, Experimental Evidence for Soliton Explosions, Phys. Rev. Lett. **88**, 073903 (2002).

[33] A. F. J. Runge, N. G. R. Broderick, and M. Erkintalo, Observation of soliton explosions in a passively mode-locked fiber laser, Optica **2**, 36 (2015).

[34] M. Liu, A.-P. Luo, Y.-R. Yan, S. Hu, Y.-C. Liu, H. Cui, Z.-C. Luo, and W.-C. Xu, Successive soliton explosions in an ultrafast fiber laser, Opt. Lett. **41**, 1181 (2016).

[35] Z.-W. Wei, M. Liu, S.-X. Ming, H. Cui, A.-P. Luo, W.-C. Xu, and Z.-C. Luo, Exploding soliton in an anomalous-dispersion fiber laser, Opt. Lett. **45**, 531 (2020).

[36] A. Komarov, A. Dmitriev, K. Komarov, D. Meshcheriakov, G. Semaan, and F. Sanchez, Theory of passively-mode-locked fiber lasers with phase-modulated square pulses, Phys. Rev. A **96**, 033820 (2017).

[37] S. K. Wang, Q. Y. Ning, A. P. Luo, Z. B. Lin, Z. C. Luo, and W. C. Xu, Dissipative soliton resonance in a passively mode-locked figure-eight fiber laser, Opt. Express **21**, 2402 (2013).

[38] K. Krzempek and K. Abramski, Dissipative soliton resonance mode-locked double clad Er:Yb laser at different values of anomalous dispersion, Opt. Express **24**, 22379 (2016).

[39] H. Ahmad, S. N. Aidita, and Z. C. Tiua, Dissipative soliton resonance in a passively mode-locked praseodymium fiber laser, Opt. Laser Technol. **112**, 20 (2019).

[40] J. Guo, S. Cundiff, J. M. Soto-Crespo, and N. Akhmediev, Concurrent Passive Mode-Locked and Self-Q-Switched Operation in Laser Systems, Phys. Rev. Lett. **126**, 224101 (2021).

[41] W. Chang, J. M. Soto-Crespo, P. Vouzas, and N. Akhmediev, Extreme amplitude spikes in a laser model described by the complex Ginzburg-Landau equation, Opt. Lett. **40**, 2949 (2015).

[42] H. J. Kbashi, M. Zajnulina, A. G. Martinez, and S. V. Sergeyev, Mulitiscale spatiotemporal structures in mode-locked fiber lasers, Laser Phys. Lett. **17**, 035103 (2020).

[43] A. Khanolkar and A. Chong, Multipulsing states management in all-normal dispersion fiber laser with a fiber-based spectral filter, Opt. Lett. **45**, 6374 (2020).

[44] A. Komarov, H. Leblond, and F. Sanchez, Quintic complex Ginzburg-Landau model for ring fiber lasers, Phys. Rev. E **72**, 025604(R) (2005).

[45] A. I. Korytin, A. Yu. Kryachko, and A. M. Sergeev, Dissipative solitons in the complex Ginzburg-Landau equation for femtosecond lasers, Radiophys. Quant. Electr. **44**, 428 (2001).

[46] J. M. Soto-Crespo, N. Akhmediev, and K. S. Chiang, Simultaneous existence of a multiplicity of stable and unstable solitons in dissipative systems, Phys. Lett. A **291**, 115 (2001).

[47] J. M. Soto-Crespo, N. Akhmediev, and G. Town, Continuous-wave versus pulse regime in a passively mode-locked laser with a fast saturable absorber, JOSA B **19**, 234 (2002).

[48] M. J. Feigenbaum, Quantitative universality for a class of nonlinear transformations, J. Stat. Phys. **19**, 25 (1978).

[49] J. M. Soto-Crespo, and N. Akhmediev, Soliton as Strange Attractor: Nonlinear Synchronization and Chaos, Phys. Rev. Lett. **95**, 024101 (2005).

[50] D. Rachinskii, A. Vladimirov, U. Bandelow, B. Hüttl, and R. Kaiser, Q-switching instability in a mode-locked semiconductor laser, J. Opt. Soc. Am. B **23**, 663 (2006).

[51] S. A. Pollack, D. B. Chang, F. A. Chudnovky, and I. A. Khakhaev, Passive Q switching and mode-locking of Er:glass lasers using $V0_2$ mirrors, J. Appl. Phys. **78**, 3592 (1995).

[52] Y.-K. Kuo, H.-M. Chen, and C.-C. Lin, A theoretical study of the Cr:$BeAl_2O_4$ laser passively Q-switched with Cr:YSO solid state saturable absorber, Chin. J. Phys. **38**, 443 (2000).